Medical & Biological Engineering & Computing (2019) 57:1591–1603
https://doi.org/10.1007/s11517-019-01983-2

ORIGINAL ARTICLE

Optic nerve head damage relation to intracranial pressure and corneal properties of eye in glaucoma risk assessment

Chingis Kharmyssov[1] · Yerkin G. Abdildin[1] · Konstantinos V. Kostas[1]

Received: 8 October 2018 / Accepted: 11 April 2019 / Published online: 26 April 2019

Abstract
This work presents results from numerical simulations of optic nerve head's (ONH) biomechanical behavior during exposure to elevated intraocular (IOP) and/or intracranial pressure (ICP) for ocular hypertension conditions. At the same time, a range of geometric and material properties of the eye structure and their interrelation with elevated IOP and ICP values are investigated. These simulations are performed on a generic model of the eye, which allows parametrical modification of geometric and material properties. Our main interest is in measuring ONH's potential damage in ocular hypertension due to intracranial pressure. Simulation results indicate a significant role of ICP in post-laminar neural tissue failure and a possible role of central corneal thickness (CCT) and scleral modulus in clinical assessment and treatment of patients with ocular hypertension (OHT). Specifically, CCT was found to affect ONH at early stages of damage in ocular hypertension conditions, and high scleral modulus seems to result in reduced shear failure in lamina cribrosa in a similar OHT state. These findings suggest that CCT could be a risk factor for glaucoma in OHT patients at initial stage along with cornea stiffness.

Keywords Ocular biomechanics · Finite element analysis · Intracranial pressure · Cornea · Glaucoma

1 Introduction

Optic nerve head (ONH), cornea, and sclera biomechanical properties are postulated to play a role in a number of ophthalmic pathologies including glaucoma, which is the second most common disease that causes blindness worldwide [1]. Glaucoma is associated with a gradual damage of the optic nerve within the ONH, where the retinal ganglion cell axons and central retinal vein pass through a collagenous meshwork, called lamina cribrosa (LC) [2, 3]. LC is known to be the site of greatest susceptibility to glaucoma disease where retinal ganglion cell dysfunction occurs [4]. The retinal ganglion cell axons pass through LC, leave the eye as a post-laminar neural tissue (PLNT), and end up in the brain while being continuously surrounded by retrobulbar cerebrospinal fluid, which exerts pressure on them (intracranial pressure (ICP)), and meninges.

Experiments have shown that high intraocular pressure (IOP) causes the axonal bundles in the LC to bow posteriorly and shear [5]. IOP greatly affects the biomechanical environment within the ONH, and high IOP values cause tissue distortions leading to glaucomatous optic neuropathy [6, 7]; however, some people have no sign of glaucoma at elevated IOP values; this state is called ocular hypertension (OHT) [8]. Recent observational [9], retrospective [10], and interventional [11] studies reported that the ocular hypertensive subjects with elevated intraocular pressure (higher than 21 mmHg) but without glaucomatous optic nerve damage had an abnormally high cerebrospinal fluid pressure. We hypothesized that the abnormally high ICP, acting as a counter pressure across the lamina cribrosa, may compensate for the elevated IOP in OHT conditions.

Glaucoma is also related to the biomechanical properties of the cornea [12] particularly for OHT patients. Although the cornea is located far from LC, which is the primary location of interest for glaucoma, corneal biomechanical properties are relevant to the rigidity and thickness of the sclera, which in turn is believed to be one of the most influential factors in LC behavior [13]. Therefore, the importance of corneal biomechanical properties should not be underestimated. Our goal is to study the influence of intracranial pressure on ONH

✉ Chingis Kharmyssov
chingis.kharmyssov@nu.edu.kz

[1] Department of Mechanical and Aerospace Engineering, Nazarbayev University, 53 Kabanbay Batyr Ave, Astana, Kazakhstan 010000

biomechanical environment in OHT patients. We have also included corneal geometric and material properties as potential factors leading to glaucoma, since central corneal thickness (CCT) was the most prone predictor for glaucoma risk assessment [14, 15] in patients with ocular hypertension. Corneal elasticity (CE) has been also shown to play a role in the interpretation of IOP, where the increased elasticity protects the eye from pressure surges [12].

Computational finite element eye models have been already successfully employed in a wide range of simulations and surgery training; see [16–18]. The novelty of this study is to use generic model to do parametric analysis, including cornea, and study the influence of intracranial pressure on optic nerve head biomechanics for ocular "hypertension" subjects using finite element analysis method. More specific to our field of study, computational finite element models have been used to study the biomechanical influence of IOP to ONH with regard to glaucoma [13, 19]. Hua et al. [20] have recently estimated the factors influencing ONH biomechanics. While IOP-induced mechanical strains on ONH have been properly characterized, the same cannot be said for ICP-induced strains on ONH, which is under-explored [21, 22]. A better understanding of IOP and its interrelations with ICP and corneal biomechanical properties is necessary in enhancing our predictions regarding glaucoma susceptibility. The contribution of this paper is twofold: (a) we characterized the effect of increased ICP and IOP on ONH's biomechanical environment for OHT subjects, using Tresca failure criterion to check whether ICP compensates the adverse effect of IOP in lamina cribrosa, and (b) we performed a parametric study to assess the effect of corneal biomechanical properties, and their interrelation with ICP, in OHT conditions, since it was hypothesized that cornea characteristics can be of importance for hypertension subjects.

2 Material and methods

In our work, a generic geometric model of the eye was constructed to perform sensitivity analysis and identify the factors influencing lamina cribrosa, via a finite element analysis approach. The selected candidate factors were systematically varied using the statistical Taguchi method; see [23]. The ONH part of the baseline eye model is identical to the one presented in [24], whereas the anterior part was constructed on the basis of the corresponding image included in [25]. The employed ocular geometry along with the design of experiments is described in detail below.

2.1 Ocular geometry

Our study involves the comparison of a series of eyeball models with varying geometric and material properties where the finite element (FE) method is employed in their assessment. A three-dimensional eyeball (see Fig. 1) was constructed in SolidWorks 2017 (Dassault Systemes, SolidWorks Corporation, Concord, MA) using dimensions for its constituting components from pertinent literature [13, 25]. The complete set of employed dimensions and material properties along with source references are included in Table 1. This model was then imported to ANSYS 15 (ANSYS, Canonsburg, PA) and automatically meshed on the basis of its geometry and the employed analysis type. Two methods were used to verify our numerical results and establish convergence: error plot checking and mesh convergence. The ANSYS error plot was used to verify stress continuity and subsequently refine the mesh when this was not accomplished. For results in convergence, we checked normal stresses, as well as error plot in ONH region, and performed mesh refinements till peak stress deviation was lower than 1%. The final employed mesh comprises 955,000 nodes and 550,000 tetrahedral and hexahedral elements (lamina cribrosa). The procedure presented in [33] was also followed here: coarse elements were first generated, and the ONH region was subsequently manually refined till convergence was reached. Our results are comparable with the ones reported in [13, 25], which also use generic eye models.

Our eye model is an extended version of the ocular model developed by Leung et al. [25] since dura mater was included to study influence of ICP, and therefore, our model is anatomically more accurate. Scleral shell thickness of the globe is assumed to be 0.8 mm with 12-mm internal radius and attenuated tapering down to 0.4 mm at canal with an angle of 30° from the vertical axis (see Fig. 1). The eye globe and adipose tissue are assumed axisymmetric around the central axis of the LC. The adipose tissue is set to cover 140° of the sclera and is modeled with a thickness of 4.6 mm [31, 32].

Lamina cribrosa thickness is set to 0.3 mm while the anterior surface radius to 0.9 mm, as described in [13]. LC is modeled as a section of a spherical shell and concentric to scleral shell. Post-laminar neural tissue, i.e., the region beneath LC, is modeled using a taper angle of 80° from the horizontal axis [13]. The PLNT starts with a retinal shell thickness of 0.24 mm and ends up with 0.2 mm at the equator while following the contour extracted from image data published in [24].

The pia and dura mater thicknesses are assumed to be 0.06 and 0.255 mm, respectively [19]. The subarachnoid space geometry follows the same image data [24] with a thickness of 0.15 mm [19] between pia and dura mater. The elastic modulus of the uniform gap (subarachnoid) between pia and dura mater was not included in the analysis as it is generally considered extremely soft [34]. The central retinal artery is modeled according to pertinent literature [19] including the effect of blood pressure. The vessel is modeled as a tube with an external wall diameter of 0.18 mm and 0.05 mm for its

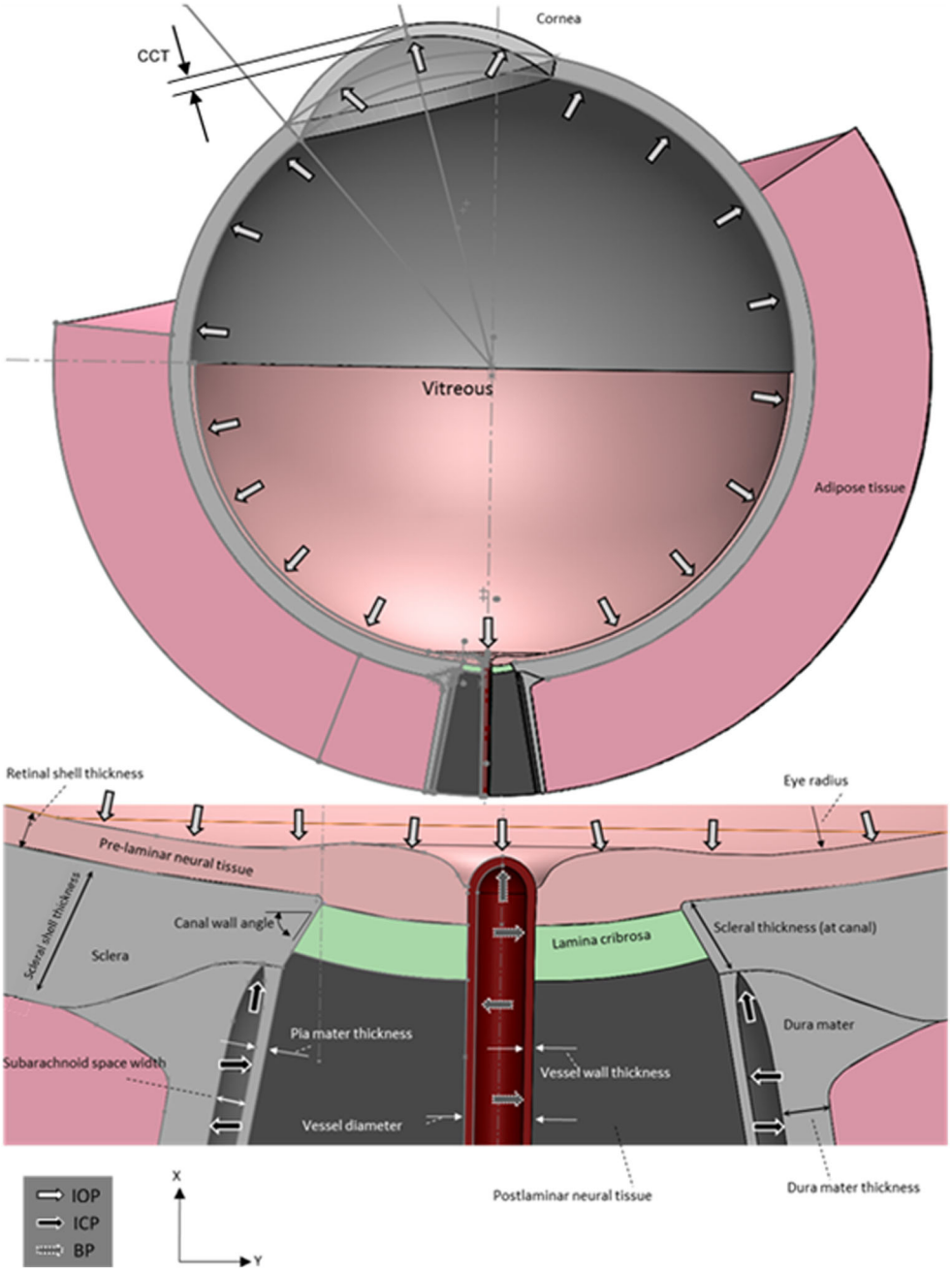

Fig. 1 FE model geometry. Top: the whole eyeball model geometry. Bottom: zoom-in view of the optic nerve head region with definitions. See Table 1 for input parameters

thickness [19]. Finally, the cornea details are set according to mean population values [28] as follows: central corneal thickness at 0.5 mm, curvature radius at 7.8 mm, and diameter at 11 mm [28]. The angle between cornea central axis and ONH central axis is set to 165°, since the blind spot is 15° nasally from the fovea [35].

All tissues are assumed as an incompressible, isotropic, linearly elastic, and homogenous material. The surface interfaces of ONH, cornea, sclera, and adipose tissue were assumed to be fully adhered, hence deforming together. Therefore, a "bonded contact" between all relevant body faces was manually applied in ANSYS Workbench in a similar fashion to [25, 36], which makes the same assumption. The baseline material properties for each tissue are adopted from literature [13, 24, 30–32], i.e., 0.29 MPa for cornea, 3 MPa for pia mater, 0.03 MPa for prelaminar and post-laminar neural tissues, 0.047 MPa for adipose tissue, 9 MPa for dura mater, and 5 MPa for artery as shown in Table 1.

2.2 Design of experiments: description and methodology

A fractional factorial design method developed by Taguchi [23] was adopted to quantitatively analyze sensitivity of

Table 1 Summary of ocular model parameters used for the eyeball model in FEA code

Parameters	Unit	Baseline value	Sources/ references
Retinal thickness	mm	0.24	[13]
LC radius (at canal)	mm	0.95	[13]
Sclera thickness at canal	mm	0.4	[26]
LC depth below rim axis	mm	0.1	[24]
LC thickness at axis	mm	0.3	[13]
Pia mater thickness	mm	0.06	[22]
Distance between pia and dura mater	mm	0.15	[19]
Dura mater thickness	mm	0.26	[19]
Vessel external diameter	mm	0.35	[19]
Vessel wall thickness	mm	0.05	[19]
Corneal radius of curvature	mm	7.8	[27]
Corneal diameter	mm	11	[28]
Central corneal thickness	mm	0.5	[28]
Central retinal artery wall thickness	mm	0.05	[19]
Central retinal artery outer diameter	mm	0.18	[19]
Subarachnoid space gap	mm	0.15	[19]
Optic nerve angle	°	80	[13]
Canal wall angle to the vertical	°	30	[13]
Peripapillary rim height	mm	0.3	[13]
IOP	mmHg	15	[19]
BP	mmHg	50	[24]
ICP	mmHg	15	[19]
CDR	–	0.45	[29]
Poisson's ratio of all materials	–	0.49	[13]
Elastic modulus of cornea	MPa	0.29	[30]
Elastic modulus of pia mater	MPa	3	[13]
Elastic modulus of prelaminar neural tissue	MPa	0.03	[13]
Elastic modulus of post-laminar neural tissue	MPa	0.03	[13]
Elastic modulus of adipose tissue	MPa	0.047	[31, 32]
Thickness of adipose tissue	mm	0.46	[31, 32]
Elastic modulus of dura mater	MPa	9	[19]
Elastic modulus of artery	MPa	5	[24]
Elastic modulus of sclera	MPa	3	[19]
Elastic modulus of lamina cribrosa	MPa	0.3	[13]

factors at two levels. The Taguchi's method facilitates system performance optimization by identifying the most important control factors allowing the use of a reduced experimental data set without compromising the efficiency of the analysis.

Our eye model's sensitivity to several factors including geometrical and material properties of its subcomponents was tested against elevated levels of ICP and IOP. Specifically, a two-level orthogonal matrix design ($L_{16}(2)^{14}$) with 14 factors was used, resulting in 16 different cases generated by Statistica (v13.3, StatSoft) software package. $L_{16}(2)^{14}$ is an orthogonal matrix design that can be represented as a two-dimensional array, where all the input factors appear in equal numbers in each vertical column and disperse evenly the pairwise combinations [37]. Here, 16 denotes the number of cases, 14 the number of factors, and *2* corresponds to the number of levels. This approach permits screening of a large number of factors and attaining good estimates of each factor's effect with a reasonably small study case set.

A total of 14 input factors were studied as summarized in Table 2. The input factors are separated into two groups. The first group includes geometric factors, whereas the second one comprises material properties. The seven geometric factors are scleral thickness at canal (A), LC radius (B), LC thickness (C), pia mater thickness (D), dura mater thickness (E), central corneal thickness (F), and retinal thickness (G). The seven material properties are scleral modulus (H), LC modulus (I),

Table 2 Input factors: geometric and material properties along with their baseline values and ranges used in the Taguchi-based sensitivity analysis

	Input factor description	Baseline value	Low level −20% value (level 1)	High level +20% value (level 2)
Geometry				
A	Scleral thickness at canal (mm)	0.4	0.32	0.48
B	Lamina cribrosa radius (at canal) (mm)	0.95	0.76	1.14
C	Lamina cribrosa thickness (mm)	0.3	0.24	0.36
D	Pia mater thickness, (mm)	0.06	0.048	0.072
E	Dura mater thickness (mm)	0.255	0.204	0.306
F	Central corneal thickness (mm)	0.5	0.4	0.6
G	Retinal thickness (mm)	0.2	0.16	0.24
Material property				
H	Sclera modulus (MPa)	3	2.4	3.6
I	Lamina cribrosa modulus (MPa)	0.3	0.24	0.36
J	Prelaminar neural tissue modulus (MPa)	0.03	0.024	0.036
K	Pia mater modulus (MPa)	3	2.4	3.6
L	Dura mater modulus (MPa)	9	7.2	10.8
M	Cornea modulus (MPa)	0.29	0.232	0.348
N	Post-laminar neural tissue modulus (MPa)	0.03	0.024	0.036

prelaminar neural tissue modulus (J), pia mater modulus (K), dura mater modulus (L), corneal modulus (M), and post-laminar neural tissue modulus (N). The factors' set was compiled to include the corneal geometric and material properties along with all other significant factors as reported in literature [24]. Each factor's value range is defined within ± 20% of the corresponding baseline value. Note that we use factorial design with two levels for multiple factors to perform a screening test in which our major concern is to identify the important factors without any detailed analysis. Furthermore, for all factors, we avoid infeasible regions and we have a typical variation used in pertinent literature [13, 24].

2.3 Optic nerve damage prediction

As indicated in [5, 38], optic nerve damage is mostly linked to shear stresses. Specifically, experimental findings show that mechanical forces, and in particular shearing stresses at LC's periphery, play a role in ONH damage [5]. In addition, computational results by Leung et al. [25] showed that Tresca criterion reasonably predicted the effect of ocular stiffening, due to aging, on optic nerve damages. The effect of radial oriented fibrils at LC's periphery, which reinforce LC against transversal shear stresses, is widely studied by computational remodeling approach [39, 40]. Therefore, in our study, we are estimating ONH damage via calculation of peak maximum shear stress values in LC and PLNT. The influence of the selected 14 input factors, for the identified 16 case studies, is reflected to the predicted peak maximum shear stresses in the LC and PLNT as shown in Table 3. Nerve damage prediction was carried out by employing the classical shear Tresca failure criterion [25, 41]. More complex damage models that account for nerve fiber anisotropy, dependence on age, and time dependence could be added, but as a first approach, the Tresca criterion appears to be sufficient since it models the observed behavior; see [25]. When local maximum shear stress in LC exceeds a threshold, the nerve is categorized as damaged. In mild ocular hypertension (corneal moduli 0.17 MPa, scleral moduli 1.84 MPa and LC stiffness 0.12 MPa, IOP 21 mmHg), nerve damage is negligible [25]. The peak MSS in LC at mild ocular hypertension was computed at 0.0032 MPa (τ_{max}); thus, we may set the Tresca criterion value (τ_c) slightly above this, i.e., 0.0035 MPa. LC shear failure corresponds to the number of nodes with MSS values higher than 0.0035 MPa and can be defined as the ratio of failure nodes over the total amount of nodes.

For the base model, an intraocular pressure of 15 mmHg is applied to the surface of the prelaminar neural tissue, sclera, and cornea. We also assume an ICP equal to 15 mmHg applied on the subarachnoid space [42] and constant arterial pressure of 55 mmHg at the vessel [43]; these values correspond to a healthy adult human.

3 Results

In this section, we present, in detail, the obtained computational results regarding the influence of ICP and corneal characteristics. The discussion begins with the effects of ICP variation, followed by the ones observed for variation in corneal geometry and material properties.

Table 3 Assignment of 14 input factors in orthogonal array and calculated peak maximum shear stress in the lamina cribrosa (LC) and post-laminar neural tissue (PLNT)

Input factors															Peak maximum shear stress (MPa) × 10^{-3}	
Case no	A	B	C	D	E	F	G	H	I	J	K	L	M	N	LC	PLNT
1	0.48	1.14	0.24	0.072	0.204	0.4	0.24	2.4	0.24	0.036	2.4	10.8	0.348	0.024	2.607	0.357
2	0.48	1.14	0.24	0.072	0.204	0.4	0.24	3.6	0.36	0.024	3.6	7.2	0.232	0.036	3.570	0.370
3	0.48	1.14	0.24	0.048	0.306	0.6	0.16	2.4	0.24	0.036	3.6	7.2	0.232	0.036	2.708	0.445
4	0.48	1.14	0.24	0.048	0.306	0.6	0.16	3.6	0.36	0.024	2.4	10.8	0.348	0.024	3.161	0.325
5	0.48	0.76	0.36	0.072	0.204	0.6	0.16	2.4	0.36	0.024	2.4	10.8	0.232	0.036	5.037	0.398
6	0.48	0.76	0.36	0.072	0.204	0.6	0.16	3.6	0.24	0.036	3.6	7.2	0.348	0.024	3.026	0.313
7	0.48	0.76	0.36	0.048	0.306	0.4	0.24	2.4	0.36	0.024	3.6	7.2	0.348	0.024	5.365	0.363
8	0.48	0.76	0.36	0.048	0.306	0.4	0.24	3.6	0.24	0.036	2.4	10.8	0.232	0.036	2.877	0.440
9	0.32	1.14	0.36	0.072	0.306	0.4	0.16	3.6	0.24	0.024	2.4	7.2	0.348	0.036	3.326	0.410
10	0.32	1.14	0.36	0.072	0.306	0.4	0.16	2.4	0.36	0.036	3.6	10.8	0.232	0.024	4.061	0.346
11	0.32	1.14	0.36	0.048	0.204	0.6	0.24	3.6	0.24	0.024	3.6	10.8	0.232	0.024	2.205	0.261
12	0.32	1.14	0.36	0.048	0.204	0.6	0.24	2.4	0.36	0.036	2.4	7.2	0.348	0.036	3.730	0.367
13	0.32	0.76	0.24	0.072	0.306	0.6	0.24	3.6	0.36	0.036	2.4	7.2	0.232	0.024	3.820	0.320
14	0.32	0.76	0.24	0.072	0.306	0.6	0.24	2.4	0.24	0.024	3.6	10.8	0.348	0.036	3.274	0.411
15	0.32	0.76	0.24	0.048	0.204	0.4	0.16	3.6	0.36	0.036	3.6	10.8	0.348	0.036	4.125	0.476
16	0.32	0.76	0.24	0.048	0.204	0.4	0.16	2.4	0.24	0.024	2.4	7.2	0.232	0.024	3.507	0.349

3.1 Effect of intracranial pressure

Table 3 clearly shows that, for all cases, shear stresses in a relatively stiff LC are considerably higher than corresponding values observed in a relatively soft PLNT. The peak MSS in LC ranges from 0.2205 to 0.5365 kPa, whereas in PLNT, it is generally much lower and varies from 0.0261 to 0.0476 kPa. Table 4 depicts collectively the results for the two factor value levels: K_n ($n = 1, 2$) corresponds to the average of eight values for each factor of the peak MSS for each factor level shown in Table 3. K_1 represents the effect of the eight low-level (i.e., − 20%) values, while K_2 represents the effect of eight high-level (i.e., + 20%) values for each factor. As an example, for input factor B (lamina cribrosa radius), $K_1 = 0.3879$ is the average of the peak MSS values in LC corresponding to $B = 0.76$ in Table 3. Range value, R, is the difference between K_1 and K_2 for each factor. Large R values signify factors with great influence on the peak MSS in LC or PLNT. Figure 2 presents a graph depicting the percentage of LC's volume subject to shear stresses above a certain value for each case in Table 3. This type of curve is helpful when computing the 95th percentile peak MSS. We should also note here that cases with a homogeneous distribution of MSS correspond to steep curves in the graph. Sensitivity analysis results are depicted in Fig. 3, where R values are plotted for each factor. Elastic moduli of LC and PLNT had the highest R values and, therefore, can be considered the most influential parameters among the selected factors. On the other hand, one may observe that although CCT is the sixth influential factor in LC, it comes second when considering PLNT shear stresses.

The relationship of peak MSS values to LC and PLNT moduli for two values of ICP and a constant IOP value (15 mmHg) is calculated and presented in Fig. 4. As can be easily seen, increasing LC modulus elevates shear stresses in it, while, conversely, the increase of ICP has a beneficial effect on shear stresses. Specifically, the low ICP value of 7 mmHg induced higher shear stresses than the higher ICP of 15 mmHg (Fig. 4a). Results from a recent computational study [19] are also indicating that ICP level affects the risk of high strains in LC and PLNT. For PLNT, the 15 mmHg ICP level induced extreme shear stresses exhibiting a more dominant effect than PLNT's stiffness (see Fig. 3b), which is consistent with findings in pertinent literature [24].

Table 4 Range analysis for the peak maximum shear stress (MSS) in lamina cribrosa (LC) and post-laminar neural tissue (PLNT)

Input factors	Peak MSS in the LC (%)			Peak MSS in the PLNT (%)		
	K_1	K_2	R	K_1	K_2	R
A	0.3506	0.3544	0.0038	0.0367	0.0376	0.0009
B	0.3879	0.3171	0.0708	0.0386	0.0360	0.0026
C	0.3346	0.3703	0.0357	0.0382	0.0362	0.002
D	0.3460	0.3590	0.013	0.0378	0.0366	0.0012
E	0.3476	0.3574	0.0098	0.0361	0.0382	0.0021
F	0.3680	0.3370	0.031	0.0389	0.0355	0.0034
G	0.3619	0.3431	0.0188	0.0383	0.0361	0.0022
H	0.3786	0.3264	0.0522	0.0379	0.0364	0.0015
I	0.2941	0.4109	0.1168	0.0373	0.0371	0.0002
J	0.3681	0.3369	0.0312	0.0361	0.0371	0.001
K	0.3508	0.3542	0.0034	0.0371	0.0373	0.0002
L	0.3631	0.3418	0.0213	0.0367	0.0377	0.001
M	0.3473	0.3577	0.0104	0.0366	0.0378	0.0012
N	0.3469	0.3581	0.0112	0.0329	0.0415	0.0086

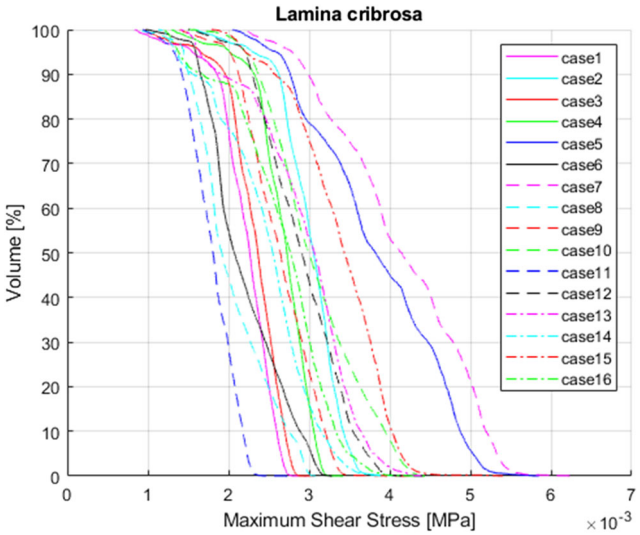

Fig. 2 Distribution of maximum shear (MSS) stresses for the 16 cases in Table 3. Each curve shows the percentage of lamina cribrosa tissue volume subject to shear stresses above a certain level

Glaucoma vision loss is also highly dependent on age and eye tissue hypertensiveness. Both IOP and elastic moduli of ocular tissues are positively correlated with age [44, 45]. Therefore, influence of IOP and ICP on LC shear failure is examined with increasing corneal, sclera, and LC moduli values (see Figs. 5 and 6). Calculated LC shear failure, using the shear failure criterion for ocular hypertension mentioned above, is depicted against varying IOP and ICP values in Fig. 5. Nerve damages increase with age due to increased stiffness of LC, sclera, and cornea. We vary the value of the elastic modulus of cornea (between 0.17 and 1.43 MPa), sclera (between 1.84 and 3.72 MPa), and lamina cribrosa (between 0.12 and 0.67 MPa) (Fig. 6) to study the effect of age stiffening [36, 44, 45]. These biomechanical ranges were adopted from experiments [36]. With a constant IOP level of 20 mmHg, when ICP level drops from 15 to 7 mmHg, LC shear failure increases from 17 to 48%. ICP seems to play the role of counter pressure to IOP in lamina cribrosa region. Abnormally low ICP (7 mmHg) induced higher translaminar pressure difference increasing LC shear failure. This is consistent with the observations of a prospective study [46], which found that cerebrospinal fluid pressure was significantly lower in glaucoma cases with normal IOP. A similar case-control study [10], including over 6000 subjects, compared ICP in patients with and without glaucoma and revealed that ICP was higher (12.6 ± 0.85 mmHg) in subjects with OHT than in age-matched control group (10.6 ± 0.81 mmHg).

3.2 Effect of corneal material and geometric properties

In this part of study, we examined shear failure for corneal thicknesses between 0.4 mm and 0.6 mm at a constant IOP value of 25 mmHg. At the same time, varying levels of LC Young's modulus, LC radius at canal, sclera Young's modulus, and sclera thickness were tested to establish the conditions revealing CCT's role. LC shear failure value for each case was calculated, and results are summarized for all examined cases in Table 5. It is easy to see that CCT value affects LC shear failure significantly in the presence of the lower-valued LC modulus and the high-valued sclera modulus. Another interesting observation in the same table can be made for scleral stiffness's effect on LS shear failure. When we consider a larger value for sclera's modulus, the expected that shear failure percentage is significantly reduced to at least half the value attained with a softer sclera. Experimental studies [47] back up this evidence as they also reveal a beneficial effect of stiffened sclera in reducing LC strain at increased IOP. Finally, [48] reported that glaucomatous eyes appear to have thinner sclera when compared with normal eyes, and this is in

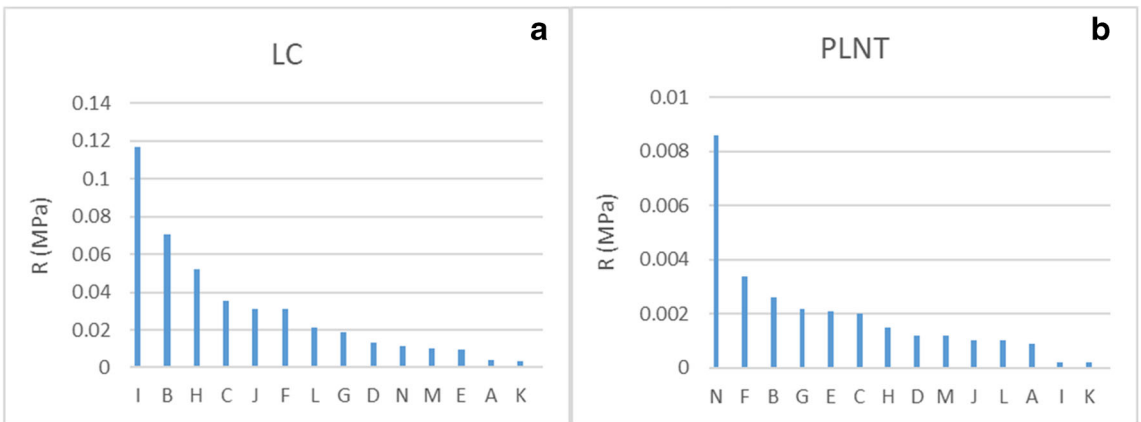

Fig. 3 Pareto chart of peak maximum shear stress (MSS) in lamina cribrosa (LC) and post-laminar neural tissue (PLNT) with respect to selected input factors: (A) scleral thickness at canal (mm), (B) lamina cribrosa radius (at canal) (mm), (C) lamina cribrosa thickness (mm), (D) pia mater thickness (mm), (E) dura mater thickness (mm), (F) central corneal thickness (mm), (G) retinal thickness (mm), (H) sclera modulus (MPa), (I) lamina cribrosa modulus (MPa), (J) prelaminar neural tissue modulus (MPa), (K) pia mater modulus (MPa), (L) dura mater modulus (MPa), (M) cornea modulus (MPa), and (N) post-laminar neural tissue modulus (MPa)

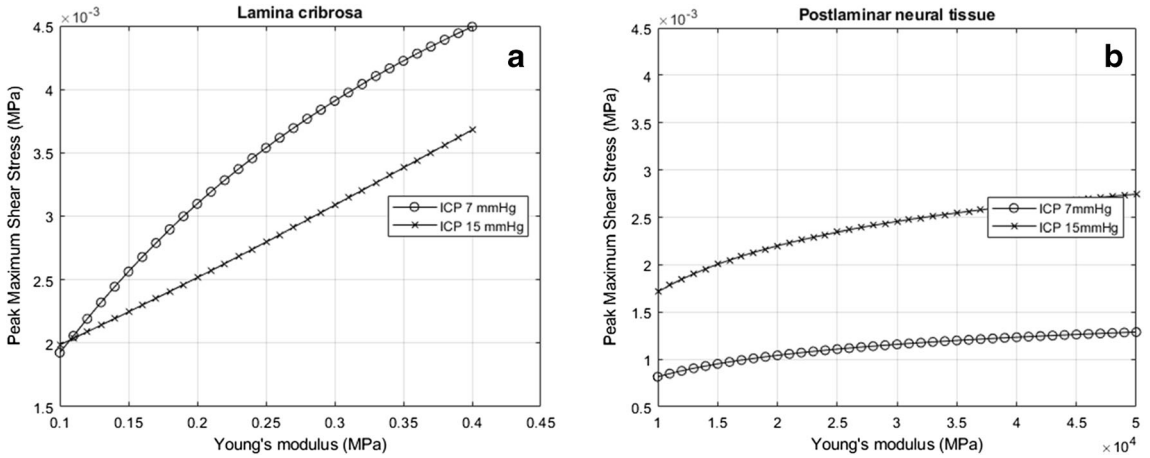

Fig. 4 Effects of variation in ICP (7 mmHg and 15 mmHg) on peak maximum shear stress as a function of stiffness for **a** LC and **b** PLNT at constant IOP value of 15 mmHg

agreement with our results, which show high LC shear failure in lower sclera thicknesses; see last two rows in Table 5.

To better illustrate the effect of the two CCT values (0.6 mm and 0.4 mm) on LC shear failure, we plot LC shear failure as a 3D surface with respect to sclera and lamina cribrosa moduli values (see Fig. 7a, b), which correspond to CCT values of 0.6 and 0.4 mm, respectively. Figure 7c, d depicts a top view of the corresponding (Fig. 7a, b, respectively) shear failure surface along with its isolines. In these figures, one may easily observe that the 10–70% isolines are shifted upwards for the larger CCT value and that the transition area between low and high failure rates is generally narrower when compared with the case of low-valued CCT. Hence, stiffer sclera and LC will generally protect the eye and especially for the case of a thicker cornea.

The isolines corresponding to 10%, 30%, and 70% of LC shear failure for both cases (CCT = 0.6 mm and CCT = 0.4 mm) are plotted side by side in Fig. 8. The green-marked areas in the subgraphs depict the difference between the same isolines for the two CCTs. One can observe that the deviation between the isolines diminishes as we approach high failure percentages, which indicated that CCT's role is more prominent and protective at low shear failure values, i.e., when ONH is starting to get damaged (initial stage).

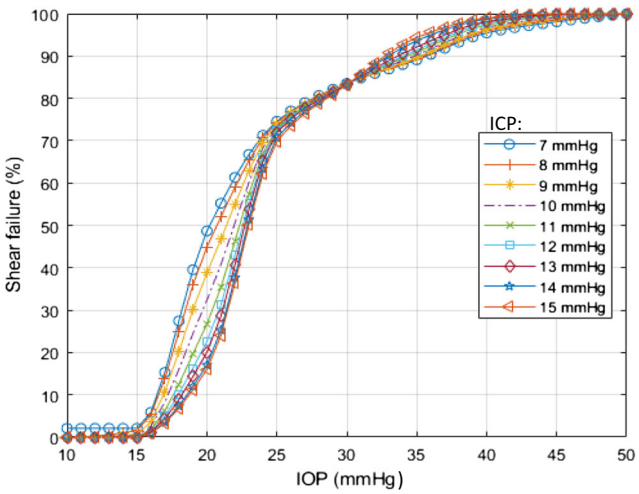

Fig. 5 Effect of variations in intraocular pressure (IOP) on shear failure in lamina cribrosa (LC) at different intracranial pressures

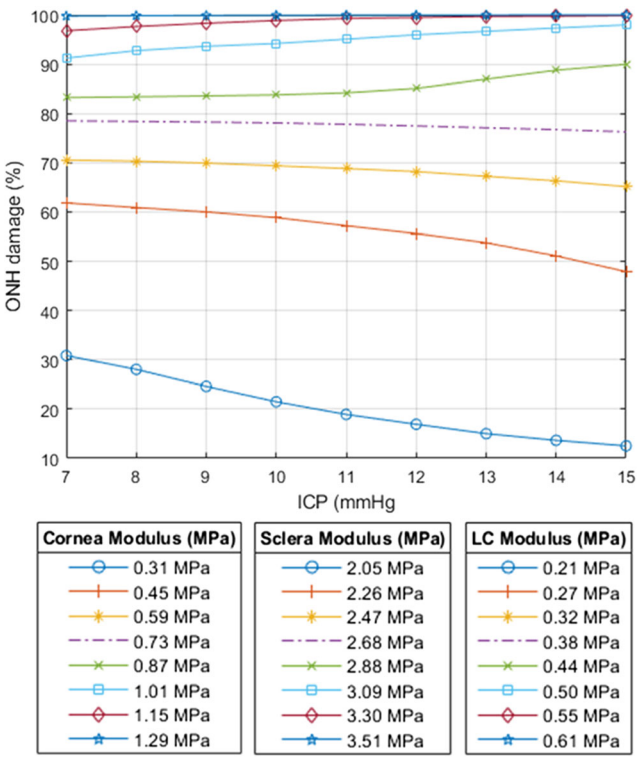

Fig. 6 Effect of intracranial pressure (ICP) on shear failure in lamina cribrosa. Elastic modulus of cornea varied from 0.31 to 1.29 MPa, sclera's elastic modulus varied in the range 1.84 to 3.72 MPa, and lamina cribrosa modulus varied between 0.12 and 0.67 MPa

Table 5 Effect of CCT variation at different range of factors on LC shear failure

Factors	± 20% Range	CCT = 0.4 mm LC shear failure (%)	CCT = 0.6 mm	Deviation (%)
LC Young's modulus (MPa)	0.24	9.87	13.20	33.74
	0.36	73.73	74.02	0.39
LC radius (at canal) (mm)	0.76	46.14	46.17	0.07
	1.14	45.30	46.60	2.87
Sclera Young's modulus (MPa)	2.4	63.85	62.95	1.41
	3.6	23.17	28.00	20.85
Sclera thickness (mm)	6.4	70.88	71.24	0.51
	9.6	21.29	21.30	0.05

4 Discussion

One of the objectives of this study was to characterize the influence of intracranial pressure on the optic nerve head for ocular hypertensive subjects. Our results suggest that optic nerve damage decreases with high intracranial pressure (15 mmHg) (Figs. 4, 5, 6) across the laminar cribrosa in ocular hypertension while inducing extra shear stresses on post laminar neural tissue. Figure 5 indicates that the higher ICP value has a beneficial effect for the whole range of LC modulus values. In this case, high intracranial pressure may act as counter pressure across the lamina cribrosa that compensates the elevated intraocular pressure. This finding agrees with suggestions from a retrospective study [10]. In contrast to the protective role of "high" intracranial pressure, three recent studies suggested that abnormally low intracranial pressure may play a role in pathogenesis of glaucomatous optic nerve damages [46, 49, 50]. Interestingly, Fig. 5 is also indicating an increase in shear failure with low ICP. One may postulate that the compensation effect of ICP leads to normal translaminar pressure difference in the eye [10, 11], while abnormally high translaminar cribrosa pressure difference can lead to

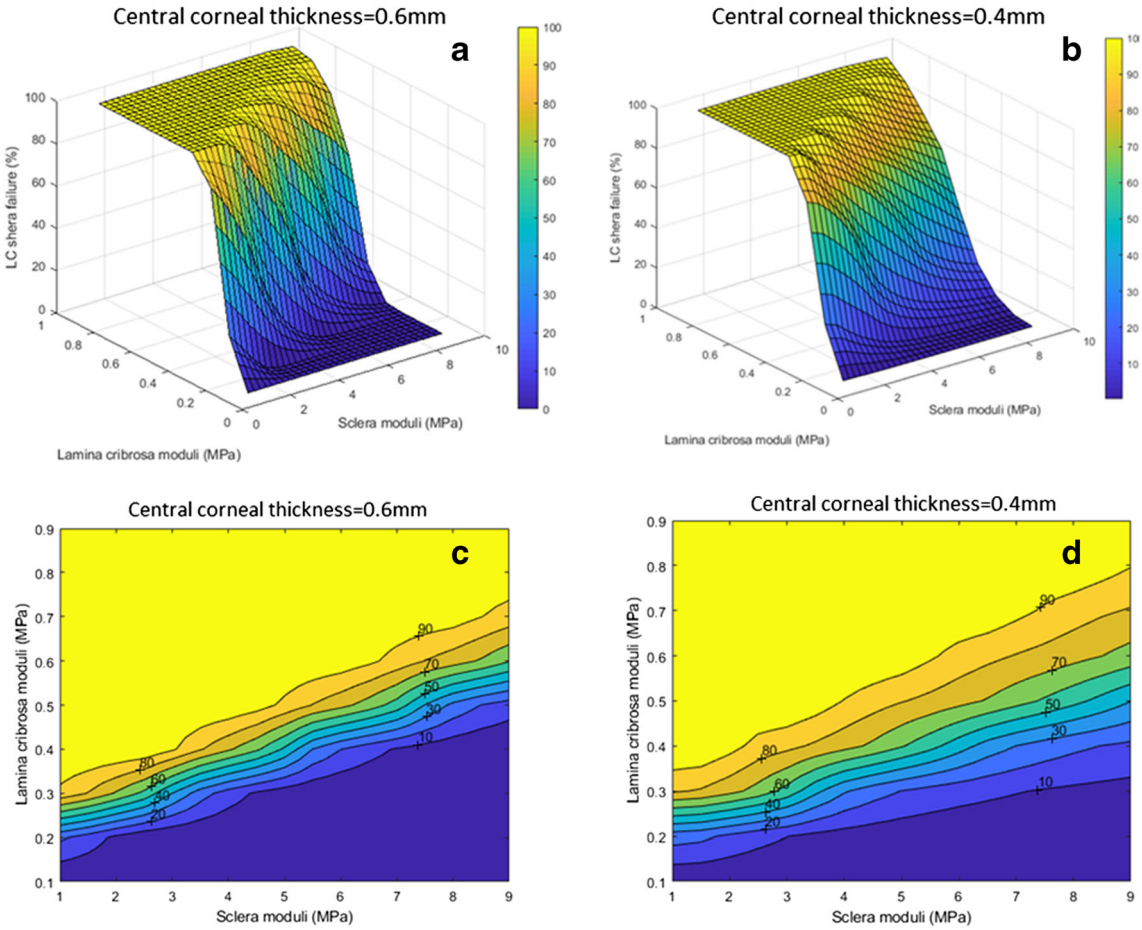

Fig. 7 Three-dimensional plots (**a**, **b**) and isolines (**c**, **d**) of LC shear failure at different levels of LC and sclera moduli. Left column results correspond to a CCT value of 0.6 mm, while the right column corresponds to the thinner cornea value of 0.4 mm

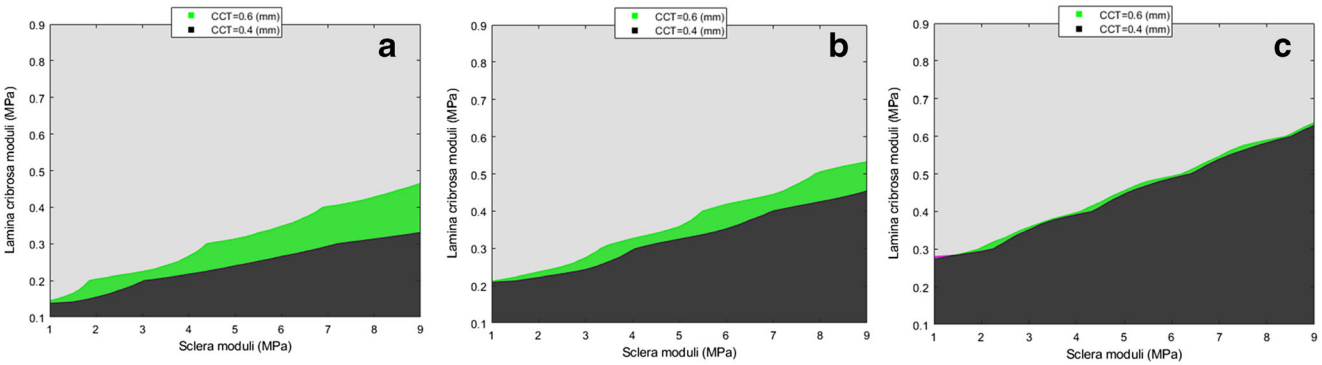

Fig. 8 Comparison of calculated shear failure isolines (**a** 10%, **b** 30%, **c** 70%) for different CCT values. Green-colored areas depict the deviation of the same failure isoline for the two corneal thicknesses (CCT = 0.4 mm and CCT = 0.6 mm). The dark-shaded area corresponds to shear failure percentages lower than the corresponding isoline's value for CCT = 0.4 mm

glaucomatous damage. If this is further verified, ocular hypertensive subjects with elevated translaminar cribrosa pressure could be treated by lowering the intraocular pressure. On the other hand, elevated levels of ICP induce extra stresses on PLNT (Fig. 4B), which is also consistent with observations from literature [19].

Glaucoma is positively correlated with IOP and age. Eye tissues stiffen with age and a positive correlation of eye's elastic moduli with age has been established in [45]. Shear failure exhibits a decrease with increasing ICP values for ocular hypertensive subjects (corneal modulus 0.31 MPa, sclera's elastic modulus 1.84 MPa and lamina cribrosa modulus 0.12 MPa) (Fig. 6). On the contrary, when LC, sclera and cornea stiffened together, the shear stress in LC slightly increased. In this range of higher-valued moduli, the ICP beneficial influence is eliminated and the estimated shear failure is even slightly higher when ICP increases. This suggests that in this area, shear failure is barely dependent on ICP values. This corroborates some studies reporting that aging would increase the shear stresses in the LC [25, 44, 45].

Brandt et al. [51] recruited 1636 patients and compared central corneal thicknesses in participants with and without glaucoma. They found out that patients with OHT had a thicker central cornea while cases with primary open-angle glaucoma exhibited thinner central corneas. Whereas studies by Johnson et al. [52], Whitacre et al. [53], and Argus et al. [54] suggest that thicker corneas may lead to IOP overestimation when measured with applanation tonometry, and OHT patients would be diagnosed with normal pressure, if corneal thickness was taken into account. Although the influence of scleral biomechanics is well established, the same cannot be said for cornea. Therefore, we tried to identify conditions in which cornea itself could be a risk factor in ocular hypertension. Specifically, we examined shear failure for corneal thicknesses between 0.4 mm and 0.6 mm at a constant IOP value of 25 mmHg. Based on our findings, a thicker CCT seems to play a protective role when it coexists with a generally stiff sclera and soft LC, and it could be the case that thicker corneas prolong glaucoma's initial stage in OHT patients with increased IOP. Since sclera and LC are embedded in the eye, monitoring and characterization of the corneal thickness and elastic modulus might be practically infeasible. On the other hand, several in vivo corneal characterization methods are developed, including mechanical indentation testing device [55], dynamic testing [56], air jet indentation testing [57, 58], ultrasound elasticity microscope [59], and ocular response analyzer [60]. Available corneal elasticity measurement methodologies could be used in glaucoma risk assessment and disease treatment management.

4.1 Limitations of the study

Our model was analyzed with linearly elastic, homogeneous, and isotropic tissues and axisymmetric geometries, which may constitute an oversimplification, as recent studies on characterization of eye tissues suggest nonlinear responses [2, 61, 62]. Nevertheless, our results refer to the immediate and average response of ONH tissues without consideration of intricate tissues' interrelations and material properties, which can justify this simplistic approach. In the same context, we acknowledge the fact that use of Tresca failure criterion will possibly omit biological and age-related axonal disruption. Another limitation of this study relates to the selection of a uniform range of variation (± 20%) for all geometric and material parameters' values. This simplifying assumption may result in a slightly distorted image regarding the significance of some factor values, which may not differ that much from the considered base values. Finally, all outcomes are considered only in terms of shear stress, whereas first and third principal strains and stresses should be also considered.

5 Conclusion

In this work, an advanced 3D eyeball model was built and employed in the investigation of several factors' contribution

to optic nerve head damage under different levels of intraocular and intracranial pressure. A range of values for intraocular and intracranial pressures was utilized to quantify optic nerve head damage in lamina cribrosa for ocular hypertension subjects. Our results indicate that intracranial pressure induces a higher shear stress on post-laminar neural tissue which does not seem to be the general case for lamina cribrosa, where intracranial pressure seems to counter balance intraocular pressure for hypertension subjects. Further to this, variations in geometric and material characteristics of eye tissues and components, including the cornea, have been demonstrated to affect lamina cribrosa and post-laminar neural tissues. For the case of cornea, our findings indicate that a thicker cornea may play a protective role of optic nerve head damage at an early stage of glaucoma in ocular hypertension subjects. However, cornea is much less influential than tissues closer to the optic nerve, such as peripapillary sclera. Future work may include modeling with patient-specific geometry from optical coherence tomography images and inclusion of non-linear material properties for eye tissues.

Funding information This work is partially supported by the Nazarbayev University individual grants 481-2018 and 445-2019.

Compliance with ethical standards

Conflict of interest The authors declare that they have no conflict of interest.

References

1. Quigley H, Broman AT (2006) The number of people with glaucoma worldwide in 2010 and 2020. Br J Ophthalmol 90(3):262–267
2. Sigal IA, Flanagan JG, Tertinegg I, Ethier CR (2009) Modeling individual-specific human optic nerve head biomechanics. Part II: influence of material properties. Biomech Model Mechanobiol 8(2):99–109. https://doi.org/10.1007/s10237-008-0119-0
3. Hattar S, Liao HW, Takao M, Berson DM, Yau KW (2002) Melanopsin-containing retinal ganglion cells: architecture, projections, and intrinsic photosensitivity. Science. 295(5557):1065–1070. https://doi.org/10.1126/science.1069609
4. Sigal IA, Ethier CR (2009) Biomechanics of the optic nerve head. Exp Eye Res 88(4):799–807
5. Yan DB, Coloma FM, Metheetrairut A, Trope GE, Heathcote JG, Ethier CR (1994) Deformation of the lamina cribrosa by elevated intraocular pressure. Br J Ophthalmol 78(8):643–648. https://doi.org/10.1136/bjo.78.8.643
6. Hernandez MR (2000) The optic nerve head in glaucoma: role of astrocytes in tissue remodeling. Prog Retin Eye Res 19(3):297–321
7. Hiraoka M, Inoue K, Ninomiya T, Takada M (2012) Ischaemia in the Zinn-Haller circle and glaucomatous optic neuropathy in macaque monkeys. Br J Ophthalmol 96(4):597–603. https://doi.org/10.1136/bjophthalmol-2011-300831
8. Burgoyne CF, Crawford Downs J, Bellezza AJ, Francis Suh JK, Hart RT (2005) The optic nerve head as a biomechanical structure: a new paradigm for understanding the role of IOP-related stress and strain in the pathophysiology of glaucomatous optic nerve head damage. Prog Retin Eye Res 24(1):39–73
9. Xie X, Chen W, Li Z, Thomas R, Li Y, Xian J, Yang D, Wang H, Zhang S, Kang Z, Wang N, the Beijing Intraocular and Intracranial Study Group (2018) Noninvasive evaluation of cerebrospinal fluid pressure in ocular hypertension: a preliminary study. Acta Ophthalmol 96(5):e570–e576. https://doi.org/10.1111/aos.13724
10. Berdahl JP, Fautsch MP, Stinnett SS, Allingham RR (2008) Intracranial pressure in primary open angle glaucoma, normal tension glaucoma, and ocular hypertension: a case-control study. Invest Ophthalmol Vis Sci 49(12):5412–5418. https://doi.org/10.1167/iovs.08-2228
11. Ren R, Zhang X, Wang N, Li B, Tian G, Jonas JB (2011) Cerebrospinal fluid pressure in ocular hypertension. Acta Ophthalmol 89(2):e142–e148. https://doi.org/10.1111/j.1755-3768.2010.02015.x
12. Johnson CS, Mian SI, Moroi S, Epstein D, Izatt J, Afshari NA (2007) Role of corneal elasticity in damping of intraocular pressure. Investig Ophthalmol Vis Sci 48(6):2540–2544. https://doi.org/10.1167/iovs.06-0719
13. Sigal IA, Flanagan JG, Ethier CR (2005) Factors influencing optic nerve head biomechanics. Investig Ophthalmol Vis Sci 46(11):4189–4199. https://doi.org/10.1167/iovs.05-0541
14. Gordon MO, Beiser JA, Brandt JD et al (2002) The ocular hypertension treatment study: baseline factors that predict the onset of primary open-angle glaucoma. Arch Ophthalmol 120(6):714–720. https://doi.org/10.1001/archopht.120.6.714
15. Herndon LW, Weizer JS, Stinnett SS (2004) Central corneal thickness as a risk factor for advanced glaucoma damage. Arch Ophthalmol 122(1):17–21
16. Lam CK, Sundaraj K, Nazri Sulaiman M (2012) Virtual simulation of eyeball and extraocular muscle reaction during cataract surgery. Procedia Engineering 41:150–155
17. Tse KM, Lee HP, Shabana N, Loon SC, Watson PG, Thean SYLH (2012) Do shapes and dimensions of scleral flap and sclerostomy influence aqueous outflow in trabeculectomy? A finite element simulation approach. Br J Ophthalmol 96(3):432–437. https://doi.org/10.1136/bjophthalmol-2011-300228
18. Lam CK, Sundaraj K, Sulaiman MN (2013) Virtual reality simulator for phacoemulsification cataract surgery education and training. Procedia Computer Science 18:742–748
19. Feola AJ, Myers JG, Raykin J, Mulugeta L, Nelson ES, Samuels BC, Ethier CR (2016) Finite element modeling of factors influencing optic nerve head deformation due to intracranial pressure. Invest Opthalmol Vis Sci 57(4):1901–1911. https://doi.org/10.1167/iovs.15-17573
20. Hua Y, Tong J, Ghate D, Kedar S, Gu L (2017) Intracranial pressure influences the behavior of the optic nerve head. J Biomech Eng 139(3):031003. https://doi.org/10.1115/1.4035406
21. I a S, Flanagan JG, Tertinegg I, Ethier CR (2004) Finite element modeling of optic nerve head biomechanics. Invest Ophthalmol Vis Sci 45(12):4378–4387. https://doi.org/10.1167/iovs.04-0133
22. Ren R, Wang N, Zhang X, Tian G, Jonas JB (2012) Cerebrospinal fluid pressure correlated with body mass index. Graefes Arch Clin Exp Ophthalmol 250(3):445–446. https://doi.org/10.1007/s00417-011-1746-1
23. Taguchi G (1986) Introduction to quality engineering: designing quality into products and processes. In: A productivity organization **(No. 658.562 T3)**
24. Hua Y, Voorhees AP, Sigal IA (2018) Cerebrospinal fluid pressure: revisiting factors influencing optic nerve head biomechanics. Invest Ophthalmol Vis Sci 59(1):154–165. https://doi.org/10.1167/iovs.17-22488
25. Leung LKK, Ko MWL, Lam DCC (2012) Effect of age-stiffening tissues and intraocular pressure on optic nerve damages. Mol Cell Biomech 9(2):157–173

26. Vurgese S, Panda-Jonas S, Jonas JB (2012) Scleral thickness in human eyes. PLoS One 7(1):e29692. https://doi.org/10.1371/journal.pone.0029692
27. Shimmyo M, Ross AJ, Moy A, Mostafavi R (2003) Intraocular pressure, Goldmann applanation tension, corneal thickness, and corneal curvature in Caucasians, Asians, Hispanics, and African Americans. Am J Ophthalmol 136(4):603–613. https://doi.org/10.1016/S0002-9394(03)00424-0
28. Ren R, Wang N, Li B, Li L, Gao F, Xu X, Jonas JB (2009) Lamina cribrosa and peripapillary sclera histomorphometry in normal and advanced glaucomatous chinese eyes with various axial length. Investig Ophthalmol Vis Sci 50(5):2175–2184. https://doi.org/10.1167/iovs.07-1429
29. Sing NM, Anderson SF, Townsend JC (2000) The normal optic nerve head. Optom Vis Sci 77(6):293–301
30. Hamilton KE, Pye DC (2008) Young's modulus in normal corneas and the effect on applanation tonometry. Optom Vis Sci 85(6):445–450. https://doi.org/10.1097/OPX.0b013e3181783a70
31. B a T, Thacker JG (1994) Three-dimensional computer model of the human buttocks, in vivo. J Rehabil Res Dev 31:111–111
32. Power E, Stitzel J, West R, Herring I (2001) A non linear finite element model of the human eye for large deformation loading. Proc. 25th … (pp. 44–45)
33. Beisheim JR, Sinclair GB (2003) On the three-dimensional finite element analysis of dovetail attachments. J Turbomach 125(2):372–379. https://doi.org/10.1115/1.1539867
34. Weller RO (2005) Microscopic morphology and histology of the human meninges. Morphologie. 89(284):22–34
35. Allingham RR, Damji K, Freedman S et al (2011) Shields textbook of glaucoma, 6th edn
36. Woo SLY, Kobayashi AS, Schlegel WA, Lawrence C (1972) Nonlinear material properties of intact cornea and sclera. Exp Eye Res 14(1):29–39. https://doi.org/10.1016/0014-4835(72)90139-X
37. McEwan W, Belavendram N, Abou-Ali M (1992) Taguchi methods and expert systems in fabrication design. Int J Press Vessel Pip 53(1):47–61. https://doi.org/10.1016/0308-0161(93)90103-Z
38. Edwards ME, Wang SSS, Good TA (2001) Role of viscoelastic properties of differentiated SH-SY5Y human neuroblastoma cells in cyclic shear stress injury. Biotechnol Prog 17(4):760–767. https://doi.org/10.1021/bp010040m
39. Grytz R, Meschke G, Jonas JB (2011) The collagen fibril architecture in the lamina cribrosa and peripapillary sclera predicted by a computational remodeling approach. Biomech Model Mechanobiol 10(3):371–382. https://doi.org/10.1007/s10237-010-0240-8
40. Grytz R, Sigal IA, Ruberti JW, Meschke G, Crawford Downs J (2012) Lamina cribrosa thickening in early glaucoma predicted by a microstructure motivated growth and remodeling approach. Mech Mater 44:99–109. https://doi.org/10.1016/j.mechmat.2011.07.004
41. Ionescu I, Guilkey JE, Berzins M, Kirby RM, Weiss JA (2006) Simulation of soft tissue failure using the material point method. J Biomech Eng 128(6):917–924. https://doi.org/10.1115/1.2372490
42. Caselli RJ, Boeve BF (2007) Textbook of clinical neurology
43. Perry RB, Rose JC (1958) The clinical measurement of retinal arterial pressure. Circulation. 18(5):864–870. https://doi.org/10.1161/01.CIR.18.5.864
44. Kiening KL, Schoening W, Unterberg AW et al (2005) Assessment of the relationship between age and continuous intracranial compliance. In: Acta Neurochirurgica, Supplementum, pp 293–297
45. Albon J, Purslow PP, Karwatowski WSS, Easty DL (2000) Age related compliance of the lamina cribrosa in human eyes. Br J Ophthalmol 84(3):318–323. https://doi.org/10.1136/bjo.84.3.318
46. Ren R, Jonas JB, Tian G, Zhen Y, Ma K, Li S, Wang H, Li B, Zhang X, Wang N (2010) Cerebrospinal fluid pressure in glaucoma. A prospective study. Ophthalmology. 117(2):259–266. https://doi.org/10.1016/j.ophtha.2009.06.058
47. Thornton IL, Dupps WJ, Roy AS, Krueger RR (2009) Biomechanical effects of intraocular pressure elevation on optic nerve/lamina cribrosa before and after peripapillary scleral collagen cross-linking. Investig Ophthalmol Vis Sci 50(3):1227–1233. https://doi.org/10.1167/iovs.08-1960
48. Norman RE, Flanagan JG, Rausch SMK, Sigal IA, Tertinegg I, Eilaghi A, Portnoy S, Sled JG, Ethier CR (2010) Dimensions of the human sclera: thickness measurement and regional changes with axial length. Exp Eye Res 90(2):277–284. https://doi.org/10.1016/j.exer.2009.11.001
49. Berdahl JP, Allingham RR, Johnson DH (2008) Cerebrospinal fluid pressure is decreased in primary open-angle glaucoma. Ophthalmology. 115(5):763–768. https://doi.org/10.1016/j.ophtha.2008.01.013
50. Jonas JB, Ritch R, Panda-Jonas S (2015) Cerebrospinal fluid pressure in the pathogenesis of glaucoma. In: Progress in brain research, vol 46, pp 67–83
51. Brandt JD, Beiser JA, Kass MA, Gordon MO (2001) Central corneal thickness in the ocular hypertension treatment study (OHTS). Ophthalmology. 108(10):1779–1788. https://doi.org/10.1016/S0161-6420(01)00760-6
52. Johnson M, Kass MA, Moses RA, Grodzki WJ (1978) Increased corneal thickness simulating elevated intraocular pressure. Arch Ophthalmol 96(4):664–665. https://doi.org/10.1001/archopht.1978.03910050360012
53. Whitacre MM, Stein RA, Hassanein K (1993) The effect of corneal thickness on applanation tonometry. Am J Ophthalmol 115(5):592–596. https://doi.org/10.1016/S0002-9394(14)71455-2
54. Argus WA (1995) Ocular hypertension and central corneal thickness. Ophthalmology. 102(12):1810–1812. https://doi.org/10.1016/S0161-6420(95)30790-7
55. Hon Y, Chen GZ, Lu SH, Lam DCC, Lam AKC (2017) In vivo measurement of regional corneal tangent modulus. Sci Rep 7(1):14974. https://doi.org/10.1038/s41598-017-14750-w
56. Soergel F, Muecke S, Pechhold W (2011) Corneal viscoelasticity spectra as a result of dynamic mechanical analysis. In: Advances in corneal research, pp 257–272
57. Zhang J, Wang L, Tian L et al (2019) Corneal biomechanical properties characterization using air-jet indentation based optical coherence tomography system (AIOCT). MATEC Web Conf 256. https://doi.org/10.1051/matecconf/201925601004
58. Alonso-Caneiro D, Kowalczyk A, Wojtkowski M et al (2011) Assessment of corneal dynamics with high-speed swept source optical coherence tomography combined with an air puff system. Opt Express 19(15):14188–14199. https://doi.org/10.1364/oe.19.014188
59. Hollman KW, Shtein RM, Tripathy S, Kim K (2013) Using an ultrasound elasticity microscope to map three-dimensional strain in a porcine cornea. Ultrasound Med Biol 39(8):1451–1459. https://doi.org/10.1016/j.ultrasmedbio.2013.02.465
60. Ramm L, Pillunat LE, Herber R et al (2019) Measurement of corneal biomechanical properties in diabetes mellitus using the ocular response analyzer and the Corvis ST. Cornea. 38:595–599. https://doi.org/10.1097/ico.0000000000001879
61. Girard MJA, Downs JC, Bottlang M et al (2009) Peripapillary and posterior scleral mechanics—part II: experimental and inverse finite element characterization. J Biomech Eng 131(5):051012. https://doi.org/10.1115/1.3113683
62. Karimi A, Razaghi R, Navidbakhsh M, Sera T, Kudo S (2017) Mechanical properties of the human sclera under various strain rates: elastic, hyperelastic, and viscoelastic models. J Biomater Tissue Eng 7(8):686–695. https://doi.org/10.1166/jbt.2017.1609

Chingis Kharmyssov is a Ph.D. candidate in Biomedical Engineering at Nazarbayev University. He received his M.Sc. degree in Medical Physics from the University of Aberdeen, Aberdeen, UK.

Konstantinos V. Kostas is an assistant professor in Mechanical and Aerospace Engineering at Nazarbayev University. His Ph.D. degree in engineering is from the National Technical University of Athens, Greece.

Yerkin G. Abdildin is an assistant professor in Mechanical and Aerospace Engineering at Nazarbayev University. He obtained a Ph.D. degree in Industrial Engineering from the University of Illinois at Urbana-Champaign.